ACI MATERIALS JOURNAL TECHNICAL PAPER

Title no. 108-M01

High-Early-Strength Engineered Cementitious Composites for Fast, Durable Concrete Repair—Material Properties

by Mo Li and Victor C. Li

The lack of durability in concrete structures worldwide demands fast and durable repairs. To address this need, high-early-strength engineered cementitious composites (HES-ECC) were recently developed for concrete repair applications in which minimum operations disruption is desired. A detailed characterization of HES-ECC's compressive, tensile, flexural, and shrinkage properties at different ages is reported in this paper. HES-ECC achieves a compressive strength of 23.59 ± 1.40 MPa (3422.16 ± 203.33 psi) in 4 hours and 55.59 ± 2.17 MPa (8062.90 ± 315.03 psi) in 28 days. Under uniaxial tension, HES-ECC exhibits tensile strain-hardening behavior with a strain capacity greater than 2.5%. Its flexural strength exceeds twice that of concrete with similar compressive strength. Under restrained shrinkage conditions, HES-ECC forms microcracks with a self-controlled crack width below 50 μm (0.002 in.). The combination of these properties suggests that HES-ECC material is highly suitable for fast and durable concrete repairs with shortened downtime and improved long-term durability.

Keywords: compressive; concrete repair; cracking; ductility; durability; flexural; high-early-strength engineered cementitious composites; shrinkage; tensile.

INTRODUCTION

Concrete structures, both new and repaired, suffer from deterioration, damage, and defects.[1-4] Concrete deteriorates over time when subjected to combined environmental (for example, freezing-and-thawing cycles, restrained shrinkage, chloride penetration, and corrosion) and mechanical (for example, fatigue) loading during service. Concrete damage is caused by short-term severe loading conditions (for example, fire, earthquakes, overloading, and impact) that result in cracking, spalling, bond splitting, or complete failure of the concrete element or structure. Concrete defects are caused by improper detailing or design, construction practices, human error, or materials with improper quality control that lead to premature deterioration or inadequate structural capacity. Concrete deterioration, damage, and defects result in a loss of durability in concrete structures, requiring efficient and effective repairs to extend their service life.[5]

Although numerous materials and techniques are used in practice to meet the demand for rapid, inexpensive, and durable concrete repairs, few address the cracking and debonding that result from the restraint of the relatively brittle repair material's shrinkage by the substrate concrete.[6] It has been estimated that almost one-half of all concrete repairs prematurely fail,[7] leading to frequent maintenance and repair throughout the structural service life, which result in significant life-cycle economic, social, and environmental impacts. For owners, the annual cost of concrete repair (including protection and strengthening) is estimated at $18 to $21 billion in the U.S. alone.[5] ASCE estimates that $2.2 trillion is needed over the next 5 years for the repair and retrofit of America's infrastructure.[8] Similarly, the repair and retrofit cost is estimated at $2 trillion for Asia's infrastructure. In Europe, Japan, Korea, and Thailand, the annual repair cost has exceeded the cost of new construction.[9] Recent life-cycle studies[10] on concrete transportation infrastructure have found that the life-cycle social costs (including construction-related congestion, operations interruption, wasted time and fuel cost, vehicle damage due to poor road conditions, and safety concerns) and environmental impacts (including raw materials and energy consumption and greenhouse gas emissions) are dominated by traffic congestion during maintenance and repair operations. The second-largest contributor to these life-cycle impacts is related to material production, the majority of which is also generated from repeated maintenance and repair operations. Resolving the challenges of durable repairs and environmental burdens of civil infrastructure requires the development of concrete repair materials with high tensile ductility that suppresses brittle fracture.

To reduce the life-cycle user and environmental impacts, there is an urgent demand for fast and durable repairs of concrete structures (for example, bridge decks, highway pavements, parking structures, and airport runways), where minimal operation disruption is needed. This requires that repair materials rapidly gain strength during early age and remain durable throughout the repaired structure's service life. For example, rapid concrete pavement repairs, including full-depth repairs and patch repairs, have become common on busy highways throughout North America.[11] Highway transportation authorities often require the repair job to be completed in 6 to 8 hours at night so the lane can be reopened to traffic the following morning. Freeways and toll roads often only permit overnight closures.[12] Overnight construction is also common for airport pavements.[13-15]

Over the past two decades, high-early-strength and fast-setting concrete materials have been successfully developed with various strength (compressive and flexural) gain rates, depending on the types of cement binders and accelerating admixtures used.[16-23] Although they possess the desired high-early-strength properties, these materials have been perceived as more prone to early-age cracking due to their higher thermal and autogenous shrinkage caused by faster early-age hydration and heat release.[24-26] Additionally, reduced freezing-and-thawing resistance[18] has also been found in some very high-early-strength concrete mixtures, limiting

ACI Materials Journal, V. 108, No. 1, January-February 2011.
MS No. M-2008-273.R2 received April 2, 2010, and reviewed under Institute publication policies. Pertinent discussion including authors' closure, if any, will be published in the November-December 2011 *ACI Materials Journal* if the discussion is received by August 1, 2011.

Mo Li *is a Research Fellow in the Department of Civil and Environmental Engineering at the University of Michigan, Ann Arbor, MI. She received her BSE from Tongji University, Shanghai, China, and her MSE and PhD from the University of Michigan. Her research interests include the development, assessment, and implementation of new material technology for structural safety, durability, and sustainability.*

ACI member **Victor C. Li** *is a Professor in the Department of Civil and Environmental Engineering at the University of Michigan. His research interests include the analysis, modeling, and design of ultraductile, green, and functional cementitious composites; their applications to innovative and sustainable infrastructure systems; and the integration of materials and structural design.*

Table 1—Mixture weight proportion of HES-Concrete and HES-ECC

Material	C*	W	S†	CA‡	HRWRA	AC	HC§	V_f‖
HES-Concrete	1.0	0.4	1.3	1.3	0.005	0.04	—	—
HES-ECC	1.0	0.33	1.0	0.064	0.0075	0.04	Optional	0.02

*Portland Type III cement.
†River sand for HES-Concrete; fine silica sand for HES-ECC.
‡Polystyrene beads as "coarse aggregates" for HES-ECC.
§Hydration control admixture is only used for HES-ECC when casting takes longer than 15 minutes after completion of mixing.
‖2 volume percent of polyvinyl alcohol fibers with 1.2% oil coating for HES-ECC.

their applications in cold regions. Achieving high-early-age strength and preventing early-age cracking are conflicting goals that must be carefully balanced through new material technology for effective concrete repairs.

The concept of simultaneously designing tensile ductility and high early strength into cementitious materials was first introduced by Wang and Li,[27] who focused on the micromechanical design of high-early-strength engineered cementitious composites (HES-ECC) using proprietary rapid-hardening cement binders. Although other binder systems (that is, Type I and Type III portland cement) were also included in the study, a detailed investigation of the effects of these binder systems on micromechanical parameters and composite properties was not conducted. Type III portland cement, however, is more widely available, less expensive, more compatible with commercially available admixtures, and more familiar to the construction industry compared to proprietary rapid-hardening cement. Building on the work of Wang and Li,[27] the systematic material development and field implementation of Type III cement-based HES-ECC, as well as the influence of a Type III portland cement binder system on cementitious matrix and fiber/matrix interfacial micromechanical parameters, are reported elsewhere.[6] This paper presents new experimental data on tensile, compressive, flexural, drying shrinkage, and restrained shrinkage cracking properties at different ages of HES-ECC using Type III cement.

RESEARCH SIGNIFICANCE

The large flow of material driven by concrete global production and consumption and the lack of durability of concrete structures have created large economic, social, and environmental impacts. A new class of repair material that achieves high-early-age strength and durability against typical cracking and delamination failures is urgently needed. This research departs from the traditionally narrow emphasis on only the high or high-early-age compressive strength of concrete repair materials but establishes a detailed understanding and database of the balanced material properties of HES-ECC. The resulting compressive strength, tensile ductility, and shrinkage-cracking resistance characteristics of the new HES-ECC are expected to contribute to fast and durable concrete repairs with a reduced environmental burden.

EXPERIMENTAL INVESTIGATION AND RESULTS

Materials

The materials' mixture compositions and proportions are shown in Table 1. A conventional concrete mixture, HES-Concrete, was used for comparison in the free shrinkage and restrained shrinkage tests. It consisted of coarse aggregate (CA) with 10 mm (0.4 in.) nominal grain size, Type III portland cement (C), river sand (S), and water (W). Type III portland cement is widely used in construction, where a more rapid strength gain rate is desirable. By grinding the cement more finely compared with Type I cement (surface area is 540 m^2/kg [2636 ft^2/kg] for Type III cement and 370 m^2/kg [1807 ft^2/kg] for Type I cement), the resultant cement surface area in contact with water increases, leading to faster hydration and strength development.[28] A high-range water-reducing admixture (HRWRA) was used to achieve sound workability. Accelerating admixtures were also included to accelerate the material's strength development and setting processes.

HES-ECC comprises Type III portland cement, water, fine silica sand, polystyrene beads, HRWRA, accelerating admixtures, and 2% (volume percentage V_f) polyvinyl alcohol (PVA) fibers. Fine silica sand has average and maximum particle sizes of 110 μm (4.33×10^{-3} in.) and 270 μm (1.06×10^{-2} in.), respectively. The fine size of silica sand was adopted to tailor matrix fracture toughness of HES-ECC for achieving multiple microcracking behavior.[6,9] Four mm (0.157 in.) polystyrene beads were incorporated to form a weak bond with the cementitious matrix to behave as an artificial flaw under tension. They were deliberately introduced into the mixture to control the initial flaw size and distribution to achieve a high density of microcracks during HES-ECC's strain-hardening stage and improve tensile ductility.[6,27]

The PVA fibers are 12 mm (0.472 in.) long and 40 μm (1.54×10^{-3} in.) in diameter and have a proprietary surface coating to control the interfacial bond between the fiber and cementitious matrix.[29] The fiber nominal tensile strength is 1620 MPa (235 ksi) and the fiber density is 1300 kg/m^3 (81 lb/ft^3).

The HES-ECC material was prepared with a Hobart-type mixer with 12 L (0.424 ft^3) capacity according to the following mixture procedure:

1. Mix Type III portland cement and silica sand for approximately 1 minute;
2. Slowly add water and continue mixing for 1 to 2 minutes;
3. Add HRWRA; continue mixing for 1 to 2 minutes until a consistent mixture is reached;
4. Slowly add PVA fibers and mix for 2 minutes until fibers are well-distributed;
5. Add polystyrene beads and mix for 1 to 2 minutes;
6. Add hydration control admixture and mix for 1 minute, unless casting will be completed within 15 minutes of completion of mixing;
7. Add accelerating admixture and mix for 1 minute before casting into molds.

The entire mixture procedure took 10 to 15 minutes for each batch. The mixture was then cast into molds with moderate vibration applied. The molds were subsequently covered with plastic sheets, demolded in 4 hours, cured in air at a room temperature of 20 ± 3°C (68 ± 4°F) and relative humidity (RH) of 40 ± 5%, and tested at different ages. The

Table 2—HES-ECC compressive, tensile, and flexural properties at different ages, mean ± standard deviation

Age	Compressive strength, MPa (psi)	Young's modulus, $\times 10^3$ MPa (ksi)	Tensile strength, MPa (psi)	Tensile strain capacity, %	Flexural strength/modulus of rupture, MPa (psi)	Deflection at failure, mm (in.)
4 hours	23.6 ± 1.4 (3422 ± 203)	13.1 ± 0.8 (1900 ± 111)	3.46 ± 0.08 (501 ± 12)	5.97 ± 0.22	9.81 ± 0.24 (1422 ± 34)	14.73 ± 0.50 (0.58 ± 0.02)
6 hours	34.2 ± 1.4 (4963 ± 181)	15.0 ± 0.8 (2173 ± 114)	4.21 ± 0.13 (610 ± 19)	4.97 ± 0.38	11.02 ± 0.36 (1599 ± 52)	15.49 ± 0.50 (0.61 ± 0.02)
12 hours	37.0 ± 1.8 (5367 ± 266)	16.1 ± 1.0 (2328 ± 147)	4.57 ± 0.17 (662 ± 25)	4.41 ± 0.33	—	—
24 hours	42.3 ± 1.4 (6129 ± 202)	18.3 ± 0.6 (2654 ± 89)	4.69 ± 0.08 (680 ± 12)	3.99 ± 0.27	11.41 ± 0.21 (1655.54 ± 30)	12.45 ± 0.50 (0.49 ± 0.02)
3 days	44.7 ± 2.4 (6482 ± 344)	19.1 ± 0.8 (2770 ± 117)	5.09 ± 0.16 (738 ± 24)	3.61 ± 0.28	12.96 ± 0.35 (1880 ± 51)	10.67 ± 0.50 (0.42 ± 0.02)
7 days	47.5 ± 1.9 (6884 ± 275)	20.6 ± 0.7 (2986 ± 101)	5.56 ± 0.11 (807 ± 16)	3.52 ± 0.29	13.55 ± 0.43 (1965 ± 63)	9.91 ± 0.30 (0.39 ± 0.01)
14 days	50.8 ± 2.4 (7366 ± 345)	22.2 ± 1.0 (3216 ± 147)	5.68 ± 0.16 (823 ± 23)	3.64 ± 0.37	—	—
28 days	55.6 ± 2.2 (8062 ± 315)	23.2 ± 1.0 (3365 ± 140)	5.68 ± 0.14 (823 ± 20)	3.47 ± 0.62	15.08 ± 0.34 (2188 ± 50)	9.91 ± 0.50 (0.39 ± 0.02)
60 days	56.8 ± 1.7 (8233 ± 250)	23.8 ± 0.7 (3452 ± 103)	5.79 ± 0.19 (839 ± 28)	3.52 ± 0.57	—	—

air-curing condition was different from ASTM standards because it was intended to simulate the curing condition in field applications, where the repair will be exposed to air and open to traffic in 4 hours.

The HEC-Concrete was mixed in a similar manner, except that fibers were not used and a 10 mm (0.394 in.) maximum-sized coarse natural/crushed aggregate was used.

Age-dependent compressive properties

Currently, there is no general standard for minimum high early strength. The New Jersey State Department of Transportation (NJDOT) specifies a minimum compressive strength of 3000 psi (20.7 MPa) in 6 hours and a minimum flexural strength of 350 psi (2.4 MPa) in 6 hours for the "fast-track mix" developed in the mid-1990s.[22] The Michigan Department of Transportation (MDOT) specifies minimum compressive strengths of 2000 psi (13.8 MPa) in 2 hours, 2500 psi (17.2 MPa) in 4 hours, and 4500 psi (31.0 MPa) in 28 days for prepackaged hydraulic fast-set materials used in structural concrete repairs.[30] Moreover, Parker and Shoemaker[21] suggested a minimum compressive strength of 2000 psi (17.2 MPa) for road-patching repair to prevent damage when initially reopened to traffic. An FHWA national research program report[31] on high-performance concretes designates three categories based on strength: (a) very early strength; (b) high early strength; and (c) very high strength. The very-early-strength concretes have a minimum compressive strength of 3000 psi (20.7 MPa) at 4 hours and the high-early-strength concretes have a minimum compressive strength of 5000 psi (34.5 MPa) at 24 hours. Additionally, the FHWA[32] recommends a minimum compressive strength of 1000 psi (6.9 MPa) at 3 hours and 3000 psi (20.7 MPa) at 24 hours for rapid-setting cementitious concretes.

Age-dependent testing in uniaxial compression was conducted to characterize HES-ECC compressive strength development as a function of material age. Compressive testing was conducted according to ASTM C39/C39M-08[33] on standard cylinders measuring 75 mm (3 in.) in diameter and 150 mm (6 in.) in length. Specimens were tested at 4, 6, 12, and 24 hours and 3, 7, 14, 28, and 60 days—measured as the time elapsed from the end of casting to the start of testing. Ten to 14 specimens were tested at each age.

Table 2 and Fig. 1(a) summarize HES-ECC's compressive strength at different ages, which reaches 23.6 ± 1.4 MPa (3422 ± 203 psi) at 4 hours, 34.2 ± 1.4 MPa (4963 ± 182 psi) at 6 hours, and 42.3 ± 1.4 MPa (6130 ± 202 psi) at 24 hours. The increasing trend slows down at later ages, leveling off at 55.6 ± 2.2 MPa (8063 ± 315 psi) at 28 days and 56.8 ± 1.7 MPa (8233 ± 250 psi) at 60 days. The average compressive strength of HES-ECC is significantly higher than the specified requirements described previously—at and beyond 4 hours—which enables the repaired structure to return to service within 4 to 6 hours after the repair job.

HES-ECC cylinder specimens exhibited very ductile failures under uniaxial compression, with gradual softening beyond the peak load and final failure planes approximately 45 degrees to the vertical axis.

The control HES-Concrete specimens were tested in the same manner and have an average compressive strength (f_c') of 49.9 MPa (7234 psi) at 7 days and 54.2 MPa (7860 psi) at 28 days.

Age-dependent tensile properties

Unlike new structures, the durability of a repaired system highly depends on the compatibility of the repair material with existing concrete.[34] Dimensional compatibility is the ability of the repair to withstand restrained volume change without cracking and loss of bond.[5] It also refers to the ability of the repair to diffuse stress concentration from existing cracks in the substrate concrete without reflective cracking. These types of cracking—either due to restrained volume change or reflective cracking—are the main causes of premature failure in concrete repairs.[35-41] To ensure dimensional compatibility with existing concrete, the repair material should be able to fully accommodate the imposed deformation that results from a combination of many factors without debonding or cracking locally. This requires the repair material to have a large tensile ductility (strain capacity) and an equal or lower elastic modulus as concrete under tension.[6] These properties must be maintained at all ages throughout the repair's life.

Age-dependent testing under uniaxial tension was conducted to measure the tensile strain capacity, Young's modulus, tensile strength, and crack width of HES-ECC at

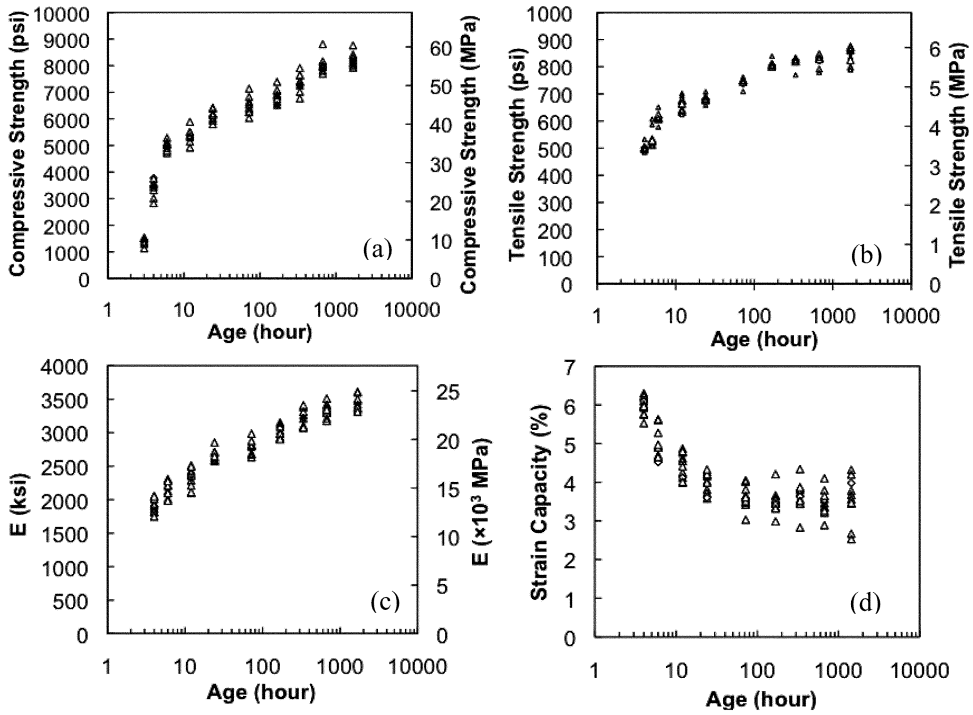

Fig. 1—Age dependency of HES-ECC compressive and tensile strength properties.

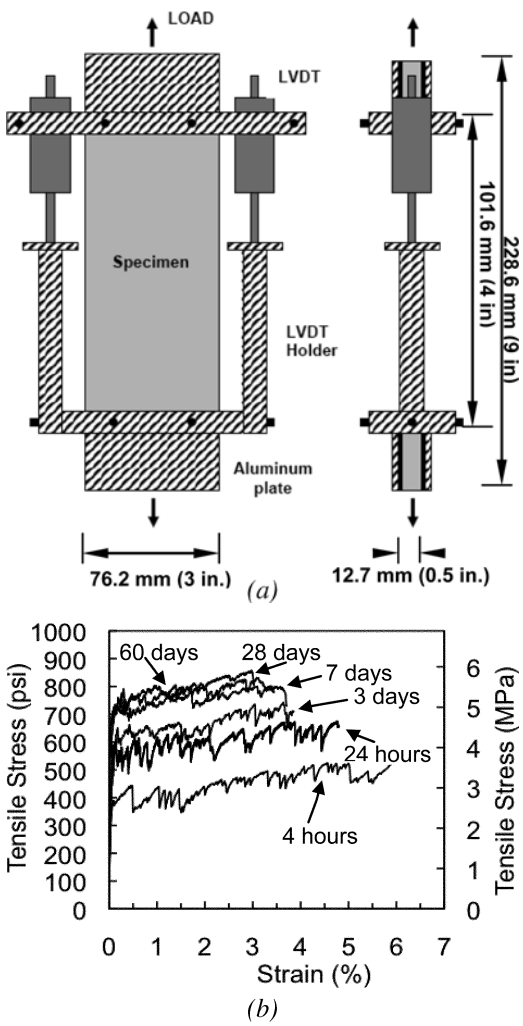

Fig. 2—Uniaxial tensile test setup and HES-ECC tensile stress-strain curve at different ages.

different ages. The direct uniaxial tensile test is considered the most convincing method for evaluating material strain-hardening behavior[42] because some quasi-brittle fiber-reinforced concrete can also show apparent hardening behavior under flexural loading—a phenomenon known as "deflection-hardening." Figure 2(a) shows the uniaxial tensile test setup and specimen dimensions. The plate specimens are 228.6 mm (9 in.) long, 76.2 mm (3 in.) wide, and 12.7 mm (0.5 in.) thick. Before testing, four aluminum plates were glued to the upper and lower faces of each end of the specimen to facilitate gripping. Tests were conducted on an MTS machine with a capacity of 25 kN (5.62 kips) under a displacement control rate of 0.005 mm/s (1.97×10^{-4} in./s). Two external linear variable displacement transducers (LVDTs) with a gauge length of 101.6 mm (4 in.) were attached to the specimen's surface to measure displacement for tensile strain computation. The MTS load cell recorded the tensile load from which the stress was computed. Specimens were tested at 4, 6, 12, and 24 hours and 3, 7, 14, 28, and 60 days—measured as the time between the end of casting and the start of testing. Ten to 14 specimens were tested at each age.

Under uniaxial tensile loading, HES-ECC exhibits significant tensile strain-hardening behavior through its unique multiple-cracking process. Figure 2(b) shows typical tensile stress-strain curves of HES-ECC from 4 hours to 60 days. Under uniaxial tension, HES-ECC first undergoes elastic straining until the first microcrack appears. The subsequent strain-hardening stage is accompanied by the formation of many closely spaced microcracks with controlled crack width. These cracks are unlike the localized fracture in concrete or other brittle materials, as they continue to carry increasing stress across the crack faces after formation. While the applied tensile deformation (or load) is increasing, the microcracks formed in HES-ECC maintain their width but increase in number until a saturated cracking state is achieved—that is, when the spacing

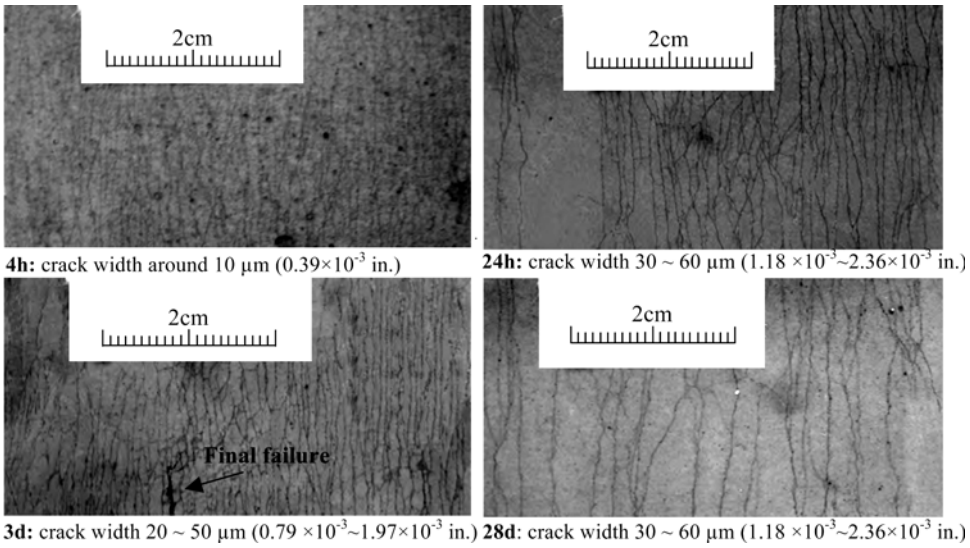

Fig. 3—HES-ECC multiple microcracking pattern on surface of uniaxial tension test specimens tested at different ages. (Note: 1 cm = 0.3937 in.)

between adjacent microcracks no longer decreases. At this point, localized fracture occurs due to exhaustion of the local fiber bridging capacity, and the HES-ECC enters the tension-softening stage. The peak stress prior to the tension-softening stage is defined as the tensile strength of the HES-ECC. The strain level corresponding to the peak stress is defined as its tensile strain capacity. The Young's modulus is determined as the slope of the line drawn between the origin and the point on the stress-strain curve corresponding to a strain of 0.015%, which is the approximate elastic strain capacity of HES-ECC.

Table 2 and Fig. 1(b) through (d) summarize the uniaxial tensile test results of HES-ECC. The tensile strength of HES-ECC rapidly increases during the first 24 hours from 3.5 ± 0.1 MPa (501 ± 12 psi) at 4 hours to 4.7 ± 0.1 MPa (680 ± 12 psi) at 24 hours. It continues increasing at a lesser rate during later ages and reaches 5.8 ± 0.2 MPa (840 ± 28 psi) at 60 days. The increase in HES-ECC's tensile strength with age is due to the hydration of the cementitious matrix and the development of the fiber/matrix interfacial bond.

The age dependency of the HES-ECC Young's modulus is plotted in Fig. 1(c). The Young's modulus of HES-ECC increases with age from 13.1 ± 0.8 GPa (1900 ± 111 ksi) at 4 hours to 23.8 ± 0.7 GPa (3452 ± 103 ksi) at 60 days. The Young's modulus of HES-ECC is generally lower than that of concrete materials due to the absence of coarse aggregates in its mixture. This lower Young's modulus is desirable for a concrete repair material because it lowers the induced tensile stress buildup caused by shrinkage restrained by the existing surrounding concrete,[7,43] thereby reducing the tendency toward cracking and repair/substrate material interface delamination.

The age-dependent development of HES-ECC's tensile strain capacity, as shown in Fig. 1(d), exceeds 5% at 4 hours, decreases to 4% at 3 days, and stabilizes to an average of 3.5% beyond 7 days (test data extend up to 60 days). The change in tensile strain capacity with age is due to the combined effects of age-dependent changes in matrix toughness and matrix/fiber interfacial properties. Regardless, the early-age and late-age tensile strain capacities of HES-ECC are several hundred times larger than the 0.01% of normal concrete materials, indicating HES-ECC's high dimensional compatibility with existing concrete.

The width of HES-ECC microcracks at the strain-hardening stage determines the material's resistance to the penetration of aggressive agents. Research has shown that a crack width less than 100 μm (3.93×10^{-3} in.) reduces water permeability[44] and chloride diffusion penetration[45] to a level equivalent to sound concrete. Figure 3 shows the multiple microcracking behavior and crack width of HES-ECC at the "saturated cracking state" at 4 hours, 24 hours, 3 days, and 28 days. To enhance the resolution of these microcrack images, epoxy glue was applied to the surfaces of the specimens before the photos were taken. Closely spaced multiple microcracks with a crack width of less than 60 μm (2.36×10^{-3} in.) were observed at all ages. It should be noted that the crack width at the very early age of 4 hours is as low as 10 μm (3.93×10^{-4} in.), whereas the tensile strain capacity is as high as 6%. This high tensile ductility and very tight crack width at an early age of HES-ECC provide a high resistance to early-age cracking due to restrained shrinkage and chloride penetration, which begins as soon as the HES-ECC repair is reopened to service.

Age-dependent flexural properties

A minimum flexural strength of the repair material, apart from its compressive strength, is usually specified as a requirement for reopening a roadway to traffic. The California Department of Transportation (Caltrans) specifies a minimum flexural strength of 400 psi (2.8 MPa) prior to opening to highway traffic for full-depth highway pavement repairs.[46] NJDOT specifies a target flexural strength of 2.4 MPa (350 psi) in 6 hours for the "fast-track mix" developed in the mid-1990s.[22] FHWA recommends a minimum flexural strength of 450 psi (3.1 MPa) for rapid-setting cementitious concretes.[33]

Age-dependent flexural testing was conducted on HES-ECC prism specimens to measure the stress-deformation curves and flexural strength (modulus of rupture [MOR]) at different ages. Flexural testing procedures followed the ASTM C78-08[47] standard. Figure 4(a) shows the third-point bending test setup and specimen dimensions. Each beam

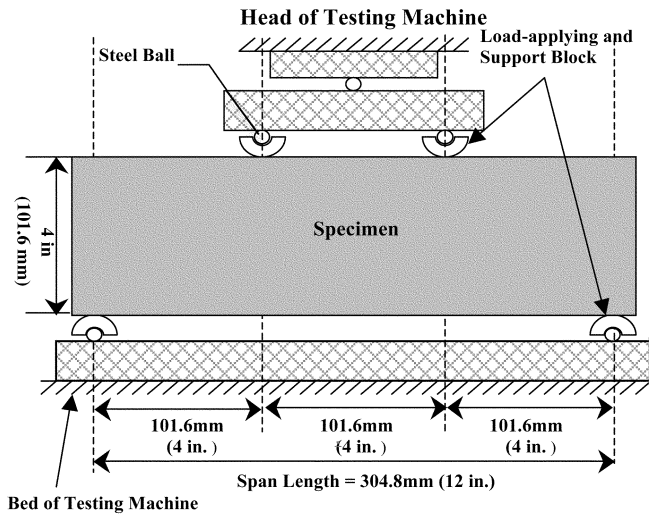

(a)

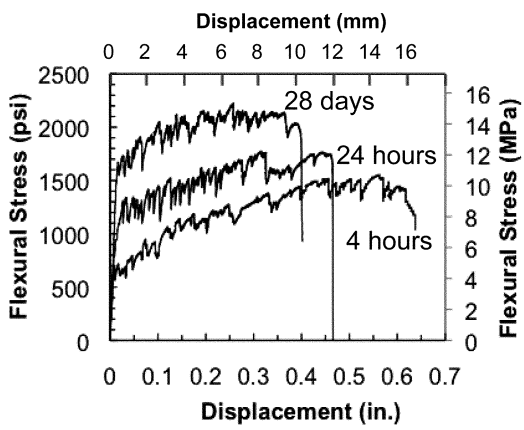

(b)

Fig. 4—Third-point bending test setup and HES-ECC flexural stress-displacement curve at different ages.

specimen measured 406.4 mm (16 in.) long, 76.2 mm (3 in.) wide, and 101.6 mm (4 in.) thick, with a test span length of 304.8 mm (12 in.). Specimens were tested at different ages from 4 hours to 60 days. The three-point bending test was conducted with an MTS machine under displacement control at a loading rate of 0.02 mm/s (7.87×10^{-4} in./s). Five specimens were tested at each age.

Table 2 summarizes the MOR and deflection at failure of HES-ECC. Figure 4(b) shows the typical flexural stress versus deflection curves of HES-ECC at 4 hours, 24 hours, and 28 days. Significant deflection-hardening behavior is observed at each age. The flexural MOR of HES-ECC rapidly increases from 9.8 ± 0.2 MPa (1422 ± 34 psi) at 4 hours to 11.4 ± 0.2 MPa (1656 ± 30 psi) at 24 hours. This increasing trend slows at later ages and reaches 15.1 ± 0.4 MPa (2188 ± 50 psi) at 28 days. Concurrently, specimen flexural ductility—defined as the maximum deflection when local failure starts—decreases after 6 hours but approaches a constant after 3 days. It should be noted that HES-ECC's flexural strength is significantly higher than NJDOT,[22] Caltrans,[46] and FHWA[32] requirements. Due to the strain-hardening behavior and tensile ductility of HES-ECC, the flexural strength of HES-ECC is more than double the flexural strength of normal concrete with similar compressive strength.

Free shrinkage properties

Drying shrinkage refers to strain caused by loss of water in hardened cementitious material.[48] Mechanisms that cause drying shrinkage of cement paste include capillary stress, disjoining pressure, and surface tension. The importance of these mechanisms depends on the RH. Capillary stress exists within a small capillary pore in the hardened cementitious matrix, where water is partially under the influence of surface interactions exerted by the pore walls. Disjointing pressure is created by the adsorption of water between C-S-H surfaces, which is the combination of steric and electrostatic forces and which increases with increasing RH and the thickness of the adsorbed water between particles. When RH < 40%, capillary stress and disjoining pressure are no longer factors; drying shrinkage is explained by significant changes in surface-free energy as the most strongly adsorbed water is removed.

Hygral deformation at a given RH can be experimentally measured as the difference between the steady-state drying shrinkage values of the dry state and the given RH. The total hygral deformation of a cementitious material can be described by the Munich model, which was originally developed for cement paste[49,50] and was later found to also work for concrete.[51] This model assumes that the capillary stress is approximately independent of the RH.[52,53] Therefore, the total hygral deformation can be described as the deformation due to a change in surface energy of C-S-H gel particles plus the deformation due to the disjointing pressure between C-S-H gel surfaces when RH > 40%.

$$\varepsilon_{hyg,\text{total}}(RH) = \varepsilon_{hyg,\text{surface-energy}}(RH) + \varepsilon_{hyg,\text{disjoining-pressure}}(RH > 40) \quad (1)$$

The first term of Eq. (1) can be expressed as

$$\varepsilon_{hyg,\text{surface-energy}}(RH) = \lambda \cdot \Delta\gamma(RH) \quad (2)$$

where λ is a function of the stiffness of the porous material.[54] The variable Δγ is the change in surface-free energy during adsorption and can be expressed as[55-57]

$$\Delta\gamma(RH) = -\frac{R \cdot T}{M \cdot A}\int_0^P \frac{u}{P}dP \quad (3)$$

where R is the universal gas constant, T is the absolute temperature, M is the mol volume of water, A is the specific surface area, P is the water vapor partial pressure that depends on RH, and u is the adsorbed water volume.

The second term of Eq. (1) can be expressed as

$$\varepsilon_{hyg,\text{disjoining-pressure}}(RH_x) = c \cdot (RH_x - RH_{40})^2 + d \cdot (RH_x - RH_{40}), \text{ for } RH \geq RH_{40} = 40\% \quad (4)$$

where c and d are empirical parameters.

Combining Eq. (1) through (4), the total hygral deformation can be rewritten as

$$\varepsilon_{hyg,\text{total}} = \lambda \cdot (A \cdot \ln(RH) + B) + c \cdot (RH_x - RH_{40})^2 + d \cdot (RH_x - RH_{40}), \text{ when } RH \geq RH_{40} = 40\%$$
$$\varepsilon_{hyg,\text{total}} = \lambda \cdot (A \cdot \ln(RH) + B), \text{ when } RH < RH_{40} = 40\% \quad (5)$$

In this study, the total hygral deformation of HES-ECC at different RHs was experimentally determined to characterize its free-drying shrinkage properties. Additionally, by fitting Eq. (5) to the experimental data, the parametric values of λ, A, B, c, and d can be determined for the physical model that describes the hygral deformation of HES-ECC.

Free-drying shrinkage tests were conducted on HES-ECC and HES-Concrete (control) prism specimens with dimensions of 200 x 40 x 40 mm (7.9 x 1.6 x 1.6 in.) in accordance with ASTM C157/C157M-99[58] and ASTM C596-01.[59] Twenty-one specimens for each mixture were cast and demolded after 24 hours. After storage at 100% RH for 2 days, three specimens of each mixture were then stored in RH = 0, 12, 33, 66, 75, 85, and 93% by using saturated salt solutions in different desiccators.[60,61] The drying shrinkage deformation and mass loss of the HES-ECC specimens was then measured as a function of drying time until hygral equilibrium was reached. After all specimens had reached hygral equilibrium, the specimens stored at 0% RH were dried in an oven at 105°C (221°F) until a constant mass was achieved. The specimens were then removed from the oven and allowed to cool down to room temperature (20 ± 1°C [66 to 70°F]). After the specimens reached thermal equilibrium with room temperature, the length changes were determined as the shrinkage values at RH = 0%.

The hygral deformation of HES-ECC and HES-Concrete is calculated as the difference between the steady-state drying shrinkage value in the dry state (0% RH) and the steady-state drying shrinkage value at specific RHs. These data are plotted as a function of RH in Fig. 5, together with the measured hygral deformation values of an ordinary ECC mixture (ECC 45) and a concrete mixture; both are Type I portland cement-based, adopted from Weimann and Li.[62] The parametric values of HES-ECC, HES-Concrete, ordinary ECC, and concrete are summarized in Table 3. The good fit between the theoretical (Eq. (5)) and experimental data demonstrated that the drying shrinkage of HES-ECC can be explained by the contraction due to the increase in surface-free energy of C-S-H particles, as well as the decrease in disjointing pressure between the surfaces of C-S-H, with the latter mechanism only operating above 40% RH. These results clarified that the drying shrinkage behavior of HES-ECC is governed by the same mechanisms as concrete materials.

The experimental results reveal that the drying shrinkage of HES-ECC is approximately twice that of the HES-Concrete control mixture and 15% higher than that of ordinary ECC. This is due to the very high cement content, finer cement particles, and the absence of a large volume of coarse aggregates and fly ash in the HES-ECC mixture. Nonetheless, Fig. 5 shows that the shrinkage strain of HES-ECC is below 0.3%, which is one order of magnitude lower than its tensile strain capacity of 3 to 6%. This implies that when the drying shrinkage of HES-ECC is restrained, the material's ductility can accommodate shrinkage deformation by forming multiple microcracks at its strain-hardening stage without localized fracture failure. After microcracking, the effective modulus of the HES-ECC will be substantially reduced, as seen in the reduced slope of the tensile stress-strain curve in the strain-hardening stage (Fig. 2(b)), thus further suppressing tensile stress buildup in the repair material due to continued restrained shrinkage. This is verified in further experimental studies in which HES-ECC drying shrinkage deformation is restrained, as described in the following section.

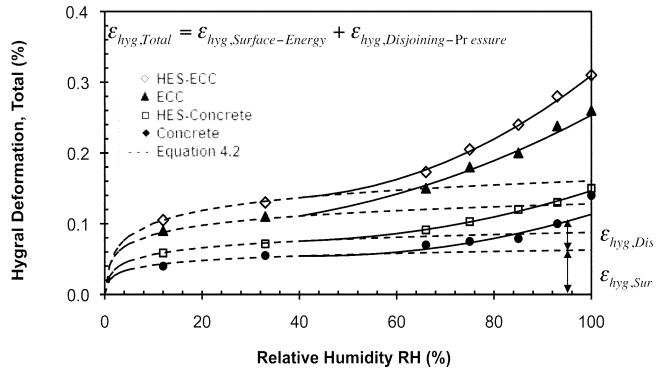

Fig. 5—Experimental data and theoretical curves of hygral deformation versus RH for investigated materials (data of HES-ECC and HES-Concrete are measured in this study; data of ECC and concrete are adopted from Weimann[51]).

Table 3—Theoretical parametric values of investigated materials

	A (J/g)	B (J/g)	λ (g/J) × 10^{-3}	c (g/J) × 10^{-5}	d (g/J) × 10^{-4}
HES-ECC	8.4	13.1	3.1	4.3	–1.0
HES-Concrete	2.9	8.5	3.8	1.6	1.2
ECC (M45)*	8.2	17.9	2.3	2.0	+7.1
Concrete*	2.3	5.1	4.0	1.9	–3.0

*Values adopted from Weimann.[51]

Restrained shrinkage properties

Due to its simplicity and versatility, the ring test has become widely used over the last two decades to measure restrained shrinkage cracking of concrete materials and fiber-reinforced cementitious composites.[63-65] It was adopted in this study to investigate the number and width of shrinkage-induced cracks in HES-ECC compared to the control HES-Concrete.

The restrained shrinkage ring test followed AASHTO PP-34-99.[66] Figure 6(a) shows the test setup and specimen dimensions. For each specimen, a 25.4 mm (1 in.) thick layer of HES-ECC or HES-Concrete material was cast around a rigid steel ring. A plastic-covered paper cylinder was used as an outer mold during casting. The outer mold was removed 4 hours after casting and the specimen was then exposed to 45 ± 5% RH and 20 ± 1°C (66 to 70°F). It should be noted that the curing conditions for the ring tests are different from the free-drying shrinkage test. The purpose of the early demolding and short (6 hours) curing time in the ring tests is to simulate the early reopening conditions in field application, whereas the free shrinkage tests employ curing conditions based on ASTM C157/C157-99[58] and ASTM C596-01[59] to characterize HES-ECC shrinkage strain at various RHs.

Once exposed to the ambient RH and temperature conditions, the drying shrinkage deformation of the HES-ECC and HES-Concrete, when restrained by the steel ring, results in internal radial pressure. Consequently, the HES-

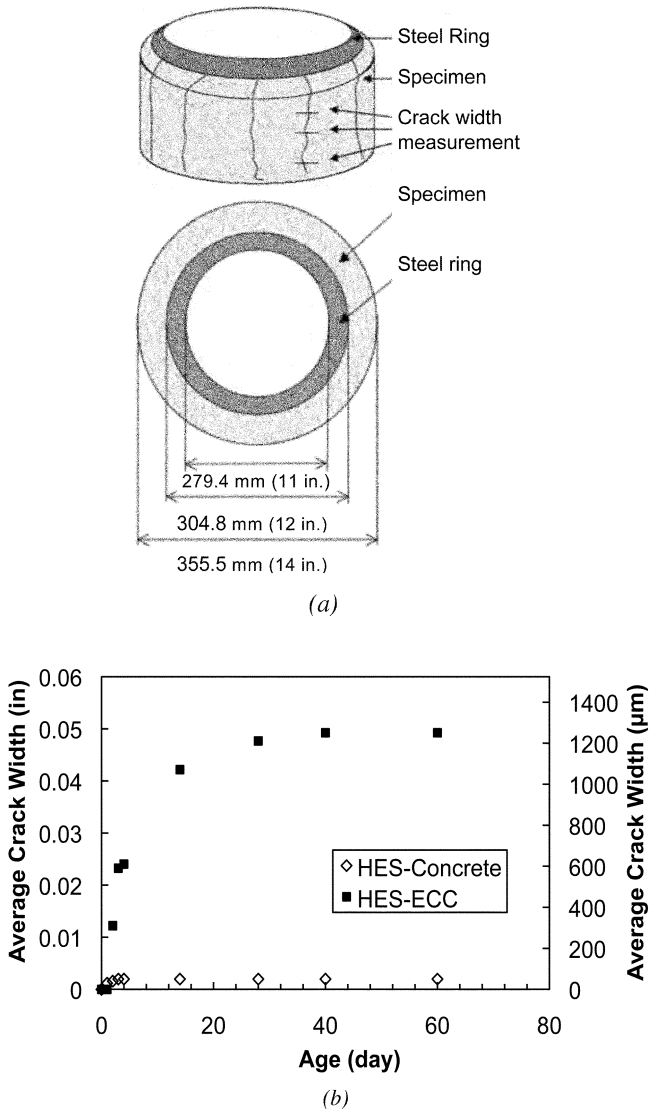

Fig. 6—Restrained shrinkage test setup, specimen dimensions, and crack width development with age.

ECC and HES-Concrete layers are subjected to a circumferential tensile stress state that can cause cracking. The cracking pattern, crack number, and crack width were measured as a function of age with a portable microscope. Measurements were taken at three different locations along each crack and the average value was plotted against time. Three HES-ECC and three HES-Concrete specimens were tested.

The test results are summarized in Fig. 6(b). For the three HES-Concrete control specimens, one localized crack was observed in each specimen. The average crack width of the three specimens was 310 μm (0.012 in.) at 2 days, 610 μm (0.024 in.) at 4 days, 1210 μm (0.048 in.) at 28 days, and 1250 μm (0.049 in.) at 60 days. For each of the three HES-ECC specimens, 25, 23, and 19 cracks had formed at 60 days. The average crack width was 40 μm (0.0016 in.) at 2 days and remained at 50 μm (0.002 in.) for the remaining test period of 2 to 60 days. These test results show that HES-ECC has significantly greater resistance to restrained shrinkage cracking than HES-Concrete despite its higher free (drying) shrinkage value. This is due to the large tensile strain capacity of HES-ECC, which leads to a negative shrinkage cracking potential (defined as the material's shrinkage strain minus its total creep, elastic, and inelastic strain capacity)[67] and results in high dimensional compatibility with existing concrete.

The cracking behavior of HES-ECC is significantly different from that of HES-Concrete. Apart from a much tighter individual crack width, as shown previously, HES-ECC retained its load-carrying capacity after crack formation. Furthermore, the transport properties between these two materials are uniquely different after crack formation. For example, Wang et al.[68] reported that as crack width increases from 100 to 500 μm (3.9×10^{-3} to 2.0×10^{-2} in.), the water permeability coefficient increases nearly 7 orders of magnitude from 1.0×10^{-11} to 1.0×10^{-4} m/s (2.54×10^{-10} to 2.54×10^{-3} in./s). For crack widths less than 100 μm (3.9×10^{-3} in.), however, the permeability coefficient remains nearly identical to that of the uncracked state, suggesting that for crack widths below this threshold, there is no significant increase in permeability after cracking. Crack widths less than 100 μm (3.9×10^{-3} in.) were also found to have the same effective chloride diffusion coefficient as uncracked concrete.[45] These observations suggest the improved transport and durability behavior of HES-ECC over HES-Concrete by virtue of its cracking behavior.

Finally, it should be pointed out that cracking in HES-ECC differs from HES-Concrete in two additional important manners—structural size and time independence. Because the width of microcracks in HES-ECC is governed by the fiber-bridging properties, it is an intrinsic material property independent of the size of structure or even of steel reinforcement details. Furthermore, the shrinkage crack width of HES-ECC becomes independent of age (drying time) once the material enters the strain-hardening stage. Furthermore, shrinkage deformation of HES-ECC will be accommodated by forming more microcracks with a controlled crack width of less than 50 μm (0.002 in.) instead of increasing the width of existing cracks (Fig. 6(b)). In contrast, continued shrinkage deformation of HES-Concrete with age is accommodated by forming localized cracks with increasing crack width. Thus, whereas the restrained shrinkage tests in this laboratory study demonstrate a 25-fold reduction in the 60-day restrained shrinkage crack width in HES-ECC compared with that in HES-Concrete, the advantage of HES-ECC can be even more significant in field repair applications.

CONCLUSIONS

This study provided a detailed understanding and database of mechanical and shrinkage properties for HES-ECC designed for rapid and durable repair of concrete structures with minimum operation disruption and long-term durability. From this study, it can be concluded that HES-ECC based on Type III portland cement possesses the following properties: (a) high-early-age compressive, flexural, and tensile strength; (b) high late-age compressive, flexural, and tensile strength; (c) large tensile ductility with controlled microcrack width; (d) a relatively low Young's modulus; and (e) a significant resistance to shrinkage-induced macrocracking.

HES-ECC attained high-early-age compressive strengths of 23.59 ± 1.40 MPa (3422 ± 203 psi) at 4 hours and 55.59 ± 2.17 MPa (8063 ± 315 psi) at 28 days. Its flexural strength was 9.81 ± 0.24 MPa (1422 ± 34 psi) at 4 hours and 15.08 ±

0.34 MPa (2188 ± 50 psi) at 28 days, which twice exceeds the flexural strength of concrete with a similar compressive strength. Its tensile strength was 3.46 ± 0.08 MPa (501 ± 12 psi) at 4 hours and 5.68 ± 0.14 MPa (823 ± 20 psi) at 28 days. The rapid strength development in HES-ECC enables the repaired concrete structure to return to service 4 to 6 hours after repair construction.

HES-ECC exhibits significant strain-hardening behavior and ductility under tension and deflection-hardening behavior under flexure. The tensile strain capacity is 2.5 to 5%—250 to 500 times that of normal concrete repair materials. During the material strain-hardening stage, HES-ECC has self-controlled tight crack widths of less than 60 μm (2.36×10^{-3} in.). The unique cracking behavior and tensile ductility of HES-ECC are crucial for achieving the long-term durability of HES-ECC repairs.

The shrinkage strain of HES-ECC was below 0.3%, which was 1 order of magnitude lower than its tensile strain capacity of 3 to 6%, therefore leading to a highly negative cracking potential value. This implied that when the drying shrinkage of HES-ECC was restrained by existing concrete, the material's ductility can accommodate shrinkage deformation by forming multiple microcracks during its strain-hardening stage without localized fracture failure. This contention was later proven by the results of the restrained shrinkage ring test, where the HES-ECC exhibited multiple microcracks, each with a width of approximately 1/25 of those of the HES-Concrete under the same RH, temperature, and other test conditions. Furthermore, the crack width in HES-ECC is independent of material age and structural dimensions.

The long-term performance of HES-ECC as a repair material should be further examined under realistic field conditions beyond laboratory studies. An HES-ECC patch repair on a bridge deck in southern Michigan was conducted in 2006. This patch is being continuously monitored. Until now, only microcracks with widths less than 60 μm (2.36×10^{-3} in.) have been found. This HES-ECC repair's long-term performance will be reported in a future article.

ACKNOWLEDGMENTS

The authors would like to graciously thank the Michigan Department of Transportation (MDOT) for partially funding this research, in particular R. Till of MDOT. The authors would also like to thank S. Wang for his advice and discussion regarding the development of HES-ECC.

REFERENCES

1. Frangopol, D. M., and Furuta, H., *Life-Cycle Cost Analysis and Design of Civil Infrastructure Systems*, ASCE, Reston, VA, 2001, 336 pp.

2. Narayan, W., "Infrastructure, Climate Change, Sustainability: The Challenge of Design—Strength or Durability," *Concrete*, V. 41, No. 9, Oct. 2007, pp. 31-33.

3. Mays, G., ed., *Durability of Concrete Structures: Investigation, Repair, Protection*, first edition, E&FN Spon, New York, 1992, 288 pp.

4. "Identifying and Evaluating Concrete Defects," http://www.cement.org/tech/cct_con_design_defects.asp. (accessed March 10, 2010)

5. Emmons, P. H., and Sordyl, D. J., "The State of the Concrete Repair Industry, and a Vision for its Future," *Concrete Repair Bulletin*, July-Aug. 2006, pp. 7-14.

6. Li, M., "Multi-Scale Design for Durable Repair of Concrete Structures," PhD dissertation, University of Michigan, Ann Arbor, MI, 2009, 425 pp.

7. Vaysburd, A. M.; Brown, C. D.; Bissonnette, B.; and Emmons, P. H., "'Realcrete' versus 'Labcrete,'" *Concrete International*, V. 26, No. 2, Feb. 2004, pp. 90-94.

8. "Report Card for America's Infrastructure," http://www.infrastructurereportcard.org/, 2009. (accessed March 10, 2010)

9. Li, V. C., "Engineered Cementitious Composites," *Proceedings of ConMat'05*, VC, Canada, Aug. 22-24, 2005, CD-documents/1-05/SS-GF-01_FP.pdf.

10. Keoleian, G. A.; Kendall, A.; Dettling, J. E.; Smith, V. M.; Chandler, R. F.; Lepech, M. D.; and Li, V. C., "Life Cycle Modeling of Concrete Bridge Design: Comparison of ECC Link Slabs and Conventional Steel Expansion Joints," *Journal of Infrastructure Systems*, ASCE, V. 11, No. 1, Mar. 2005, pp. 51-60.

11. American Concrete Pavement Association, "How Do I Obtain 'High Early Strength' Concrete?" http://www.pavement.com/Concrete_Pavement/Technical/FATQ/Design High_Early_Strength_Concrete.asp. (accessed March 10, 2010)

12. Delatte, N. J., *Concrete Pavement Design, Construction, and Performance*, E&FN Spon, New York, 2007, 392 pp.

13. Portland Cement Association, http://www.cement.org/pavements/pv_cp_airports.asp. (accessed on August 15, 2009)

14. Elhindy, E.; Chevalier, F.; and Khayat, K. H., "Airfield Pavement Repair Using High Early Strength Concrete: Experience of the Aeroports De Montreal," *Concrete for Infrastructure and Utilities*, L. D. Ravindra and N. A. Henderson, eds., E&FN Spon, New York, 1996, pp. 601-603.

15. Kohn, S. D.; Tayabji, S.; and Okamoto, P., *Best Practices for Airport Portland Cement Concrete Pavement Construction Rigid Airport Pavement*, American Concrete Pavement Association, Washington, DC, 2003, 146 pp.

16. Seehra, S. S.; Gupta, S.; and Kumar, S., "Rapid Setting Magnesium Phosphate Cement for Quick Repair of Concrete Pavements—Characterization and Durability Aspects," *Cement and Concrete Research*, V. 23, No. 2, 1993, pp. 254-266.

17. Knofel, D., and Wang, J. F., "Properties of Three Newly Developed Quick Cements," *Cement and Concrete Research*, V. 24, No. 5, 1994, pp. 801-812.

18. Whiting, D., and Nagi, M., "Strength and Durability of Rapid Highway Repair Concretes," *Concrete International*, V. 16, No. 9, Sept. 1994, pp. 36-41.

19. Sprinkel, M. M., "Very-Early-Strength Latex-Modified Concrete Overlay," *Report* No. VTRC99-TAR3, Virginia Department of Transportation, Richmond, VA, 1998, 11 pp.

20. Baraguru, P. D., and Bhatt, D., "Rapid Hardening Concrete," *Report* No. FHWA NJ 2001-3, New Jersey Department of Transportation, Trenton, NJ, 2000, 22 pp.

21. Parker, F., and Shoemaker, M. L., "PCC Pavement Patching Materials and Procedures," *Journal of Materials in Civil Engineering*, ASCE, V. 3, No. 1, 1991, pp. 29-47.

22. Kurtz, S.; Balaguru, P.; Consolazio, G.; and Maher, A., "Fast Track Concrete for Construction Repair," *Report* No. FHWA 2001-015, New Jersey Department of Transportation, Trenton, NJ, 1997, 67 pp.

23. Anderson, J.; Daczko, J.; and Luciano, J., "Producing and Evaluating Portland Cement-Based Rapid Srength Concrete," *Concrete International*, V. 25, No. 8, Aug. 2003, pp. 77-82.

24. Bentz, D. P., and Peltz, M. A., "Reducing Thermal and Autogeneous Shrinkage Contributions to Early-Age Cracking," *ACI Materials Journal*, V. 105, No. 4, July-Aug. 2008, pp. 414-420.

25. Mehta, P. K., and Burrows, R. W., "Building Durable Structures in the 21st Century," *Concrete International*, V. 23, No. 3, Mar. 2001, pp. 57-63.

26. Mihashi, H.; Nishiyama, N.; Kobayashi, T.; and Hanada, M., "Development of a Smart Material to Mitigate Thermal Stress in Early Age Concrete," *Control of Cracking in Early Age Concrete*, H. Mihashi and F. H. Wittmann, eds., Balkema, Rotterdam, 2002, pp. 385-392.

27. Wang, S., and Li, V. C., "High Early Strength Engineered Cementitious Composites," *ACI Materials Journal*, V. 103, No. 2, Mar.-Apr. 2006, pp. 97-105.

28. Neville, A. M., and Brooks, J. J., *Concrete Technology*, Prentice Hall, Upper Saddle River, NJ, 1987, 456 pp.

29. Li, V. C.; Wu, C.; Wang, S.; Ogawa, A.; and Saito, T., "Interface Tailoring for Strain-Hardening PVA-ECC," *ACI Materials Journal*, V. 99, No. 5, Sept.-Oct. 2002, pp. 463-472.

30. MDOT, "Qualification Procedure For Prepackaged Hydraulic Fast-Set Materials for Patching Structural Concrete," MDOT Quality Assurance and Quality Control (QA/QC), Michigan Department of Transportation, Lansing, MI, 2003.

31. Zia, P.; Leming, M. L.; and Ahmad, S. H., "High Performance Concretes—A State-of-the-Art Report," *Report* No. SHRP-C/FR-91-103, Strategic Highway Research Program, National Research Program, Washington, DC, 1991, 251 pp.

32. FHWA, "Manual of Practice: Materials and Procedures for Rapid Repair of Partial-Depth Spalls in Concrete Pavements," Federal Highway Administration, Washington, DC, 1999, 135 pp.

33. ASTM C39/C39M-09a, "Standard Test Method for Compressive Strength of Cylindrical Concrete Specimens," ASTM International, West Conshohocken, PA, 2009, 7 pp.

34. Morgan, D. R., "Compatibility of Concrete Repair Materials and Systems," *Construction and Building Materials*, V. 10, No. 1, 1996, pp. 57-67.

35. Czarnecki, L.; Garbacz, A.; Lukowski, P.; and Clifton, J. R., "Polymer Composites for Repairing Portland Cement Concrete: Compatibility Project," *Technical Report* NISTIR 6394, National Institute of Standards and Technology, Gaithersburg, MD, 1999, 87 pp.

36. Emmons, P. H.; Vaysburd, A. M.; Poston, R. W.; and McDonald, J. E., "Performance Criteria for Concrete Repair Materials, Phase II, Field Studies," *Technical Report* REMR-CS-60, U.S. Army Waterways Experiment Station, Vicksburg, MS, Sept. 1998, 98 pp.

37. Pigeon, M., and Bissonnette, B., "Bonded Concrete Repairs: Tensile Creep and Cracking Potential," *Concrete International*, V. 21, No. 11, Nov. 1999, pp. 31-35.

38. Vaysburd, A. M., "Research Needs for Establishing Material Properties to Minimize Cracking in Concrete Repairs, Summary of a Workshop," *ICRI Publication No.* Y320001, 1996, 32 pp.

39. Tayabji, S. D., and Okamoto, P. A., "Thickness Design of Concrete Resurfacing," *Proceedings of the 3rd International Conference on Concrete Pavement Design and Rehabilitation*, Purdue University, West Lafayette, IN, 1985, pp. 367-379.

40. ERES Consultants, Inc., "Evaluation of Unbonded Portland Cement Concrete Overlays," *NCHRP Report* 415, Transportation Research Board, Washington, DC, 1999, 88 pp.

41. Huang, Y. H., *Pavement Analysis and Design*, second edition, Prentice Hall, Upper Saddle River, NJ, 2003, 792 pp.

42. Stang, H., "Scale Effects in FRC and HPRFCC Structural Elements," *High Performance Fiber Reinforced Cementitious Composites, RILEM Proceedings Pro 30,* A. E. Naaman and H. W. Reinhardt, eds., 2003, pp. 245-258.

43. Li, M., and Li, V. C., "Durability of HES-ECC Repair under Mechanical and Environmental Loading Conditions," *Proceedings, High Performance Fiber Reinforced Cement Composites*, H. W. Reinhardt and A. E. Naaman, eds., Mainz, Germany, 2007, pp. 399-408.

44. Lepech, M. D., and Li, V. C., "Water Permeability of Engineered Cementitious Composites," *Journal of Cement and Concrete Composites*, V. 31, No. 10, 2009, pp. 744-753.

45. Sahmaran, M.; Li, M.; and Li, V. C., "Transport Properties of Engineered Cementitious Composites under Chloride Exposure," *ACI Materials Journal*, V. 104, No. 6, Nov.-Dec. 2007, pp. 604-611.

46. Anderson, J., "Paving Repair Finds a Four-Hour Champion," *Concrete Construction*, V. 46, No. 12, 2001, pp. 69-70.

47. ASTM C78-08, "Standard Test Method for Flexural Strength of Concrete (Using Simple Beam with Third-Point Loading)," ASTM International, West Conshohocken, PA, 2008, 4 pp.

48. Mindess, S.; Young, J. F.; and Darwin, D., *Concrete*, second edition, Prentice Hall, NJ, 2003, 644 pp.

49. Wittmann, F. H., "The Structure of Hardened Cement Paste—A Basis for a Better Understanding of the Materials Properties," *Hydraulic Cement Paste: Their Structure and Properties*, Cement and Concrete Association, Slough, UK, 1976, pp. 96-117.

50. Wittmann, F. H., "Creep and Shrinkage Mechanisms," *Creep and Shrinkage in Concrete Structures*, Z. Bažant and F. H. Wittmann, eds., John Wiley & Sons, Inc., New York, 1982, pp. 129-161.

51. Weimann, M. B., "Vergleichende Studie der hygrischen Eigenschaften ausgewählter Werkstoffe des Bauwesens," *Building Materials Reports No. 14*, Aedificatio Verlag GmbH, Freiburg, Germany, 2001, 150 pp.

52. Beltzung, F.; Wittmann, F. H.; and Holzer, L., "Influence of Composition of Pore Solution on Drying Shrinkage," *Creep, Shrinkage and Durability Mechanics of Concrete and other Quasi-Brittle Materials*, F. J. Ulm; Z. P. Bažant; and F. H. Wittmann, eds., Elsevier Science Ltd., Cambridge, MA, 2001, pp. 39-48.

53. Schubert, H., *Kapillarität in porösen Feststoffsystemen*, Springer-Verlag, Berlin, Germany, 1982, 350 pp.

54. Hiller, K. H., "Strength Reduction and Length Changes in Porous Glass Caused by Water Vapour Adsorption," *Journal of Applied Physics*, V. 35, No. 5, 1964, pp. 1622-1628.

55. Yates, D. J. C., "Molecular Specificity in Physical Adsorption," *Advances in Catalysis and Related Subjects*, V. 12, 1960, pp. 265-312.

56. Flood, E. A., and Heyding, R. D., "Stresses and Strains in Adsorbent-Adsorbate Systems," *Canadian Journal of Chemistry*, V. 32, 1954, pp. 660-682.

57. Wittmann, F. H., "Surface Tension, Shrinkage and Strength of Hardened Cement Paste," *Materials and Structures*, V. 1, No. 6, 1968, pp. 547-552.

58. ASTM C157/C157M-99, "Standard Test Method for Length Change of Hardened Hydraulic-Cement, Mortar, and Concrete," ASTM International, West Conshohocken, PA, 1999, 7 pp.

59. ASTM C596-01, "Standard Test Method for Drying Shrinkage of Mortar Containing Hydraulic Cement," ASTM International, West Conshohocken, PA, 2001, 3 pp.

60. Wittmann, F. H., and Martinola, G., "Decisive Properties of Durable Cement-Based Coatings for Reinforced Concrete Structures," *International Journal for Restoration of Buildings and Monuments*, V. 9, No. 3, 2003, pp. 235-264.

61. Greenspan, L., "Humidity Fixed Points of Binary Saturated Aqueous Solutions," *Journal of Research of the National Bureau of Standard—American Physics Chemistry*, V. 81A, No. 1, Jan.-Feb. 1977, pp. 89-96.

62. Weimann, M. B., and Li, V. C., "Hygral Behavior of Engineered Cementitious Composites (ECC)," *International Journal for Restoration of Buildings and Monuments*, V. 9, No. 5, 2003, pp. 513-534.

63. Weiss, W. J., and Ferguson, S., "Restrained Shrinkage Testing: The Impact of Specimen Geometry on Quality Control Testing for Material Performance Assessment," *Concreep 6: Creep, Shrinkage, and Curability Mechanic of Concrete and Other Quasi-Brittle Materials*, F. J. Ulm; Z. P. Bažant; and F. H. Wittman, eds., Elsevier, Cambridge, MA, 2001, pp. 645-651.

64. Shah, S. P.; Karaguler, M. E.; and Sarigaphuti, M., "Effects of Shrinkage-Reducing Admixtures on Restrained Shrinkage Cracking of Concrete," *ACI Materials Journal*, V. 89, No. 3, May-June 1992, pp. 291-295.

65. Bentur, A., and Mindess, S., *Fibre Reinforced Cementitious Composites*, E&FN Spon, New York, 1990, 449 pp.

66. AASHTO PP 34-99, "Standard Practice for Estimating the Cracking Tendency of Concrete," American Association of State Highway and Transportation Officials, Washington, DC, 1999, 5 pp.

67. Li, M., and Li, V. C., "Influence of Material Ductility on the Performance of Concrete Repair," *ACI Materials Journal*, V. 106, No. 5, Sept.-Oct. 2009, pp. 419-428.

68. Wang, K.; Jansen, D.; Shah, S.; and Karr, A., "Permeability Study of Cracked Concrete," *Cement and Concrete Research*, V. 27, No. 3, 1997, pp. 381-393.